Applied Physics Express

LETTERS

Beam control of high-power broad-area photonic crystal lasers using ladderlike groove structure

Applied Physics Express **10**, 062701 (2017)
https://doi.org/**10.7567/APEX.10.062701**

Beam control of high-power broad-area photonic crystal lasers using ladderlike groove structure

Tao Wang[1,2], Lijie Wang[1], Shili Shu[1], Sicong Tian[1], Zefeng Lu[1,2], Guanyu Hou[1,2], Huanyu Lu[1,2], Cunzhu Tong[1]*, and Lijun Wang[1]

[1]*State Key Laboratory of Luminescence and Applications, Changchun Institute of Optics, Fine Mechanics and Physics, Chinese Academy of Sciences, Changchun 130033, China*
[2]*University of Chinese Academy of Sciences, Beijing 100049, China*

*E-mail: tongcz@ciomp.ac.cn

Received February 21, 2017; accepted April 19, 2017; published online May 8, 2017

The high-power broad-area (BA) photonic bandgap crystal (PBC) diode laser is promising as a high-brightness laser source, however, it suffers from poor lateral beam quality owing to the intrinsic drawback of BA lasers. In this paper, a ladderlike groove structure (LLGS) was proposed to improve both the lateral beam quality and emission power of BA PBC lasers. An approximately 15.4% improvement in output power and 25.2% decrease in the lateral beam parameter product (BPP) were realized and the underlying mechanism was discussed. On the basis of the one-dimensional PBC epitaxial structure, a stable vertical far field was demonstrated. © 2017 The Japan Society of Applied Physics

There is an increasing demand for high-power and high-beam-quality diode lasers for applications such as material processing, pumping solid-state lasers or fiber lasers, and defense. Recently, diode lasers based on the one-dimensional photonic bandgap crystal (PBC) structure have been proposed and developed[1–5] to improve the beam quality of diode lasers. Low vertical divergence and circular beams[5] have been demonstrated in single devices, providing a potential solution for the intrinsic drawbacks of diode lasers, i.e., high divergence and elliptical beam shape. The PBC lasers can be designed to allow fundamental transverse-mode operation even at high output power. The thick waveguide of PBC lasers reduces the optical power density and thus pushes back the onset of the catastrophic optical mirror damage (COMD) limit. However, the PBC lasers suffer from the same issue as common broad-area (BA) diode lasers,[6] i.e., poor beam quality in the lateral direction. The large number of high-order lateral modes deteriorates the lateral divergence, hence hindering many underlying applications and limiting the improvement of efficiency. To improve the lateral beam quality of BA diode lasers, numerous methods have been proposed, including a tapered waveguide,[7] tilted cavity,[8] phase structure,[9,10] resonant antiguiding,[11] and external cavity techniques.[12] However, the improvement of lateral beam quality is often accompanied by either sacrificing output power or an increased processing complexity, as well as the cost of these methods.

In our previous work,[13] we demonstrated that a fish-bone-shaped microstructure fabricated on PBC BA lasers was able to reduce the lateral divergence without penalizing the emission power. The mode-filtering function of the microstructure contributes to an improvement in the lateral divergence. However, there is still much room for the improvement of both the lateral beam quality and the output power of PBC BA lasers. It had been demonstrated that the control of the lateral index difference[14] and the suppression of carrier accumulation at the device edges[15] play an important role in the improvement of lateral beam quality. In this work, a ladderlike groove structure (LLGS) was introduced to BA PBC lasers to improve both the beam quality and the output power by reducing current diffusion and modifying the lateral index difference. The modal behavior and the impact on output power were investigated in detail, and the near-field (NF) and far-field (FF) characteristics were compared.

The schematic diagram of the BA PBC laser with the LLGS is shown in Fig. 1, and the inset in Fig. 1 shows a cross-sectional scanning electron microscopy (SEM) image of the actual fabricated LLGS waveguide. To investigate the effect of the LLGS on the BA PBC laser, we calculated the carrier density and intensity profile using the LASTIP software,[16] which allows self-consistent simulation of multi-mode wave guiding, drift diffusion of carriers, and heat flow in stripe lasers. Because of the symmetry of the LLGS, only half the structure was simulated in the lateral direction. The whole structure of the LLGS laser can be divided into five regions for simplified understanding. Regions I and II are, respectively, the injection and insulation areas. Region III is the etched grooves near the stripe edges. Region V is the bottom groove. Region IV is the shoulder between regions III and V. Figure 2 shows the calculated carrier-density profile in the upper quantum well (QW) in the standard and LLGS lasers. The etched p-cap layer and the heavily doped layers (Region III) determine the injection profile.[17] As shown in Fig. 2, the lateral current spread is suppressed because of the thick waveguide and the low doping profile at the ladder ($\sim 5 \times 10^{17}\,\mathrm{cm}^{-3}$), which results in a much lower carrier density in Region III of the LLGS ($\sim 1.2 \times 10^{17}\,\mathrm{cm}^{-3}$) than that of standard lasers ($\sim 1.8 \times 10^{17}\,\mathrm{cm}^{-3}$). This means improved localized Joule heating[18] and decreased lateral carrier accumulation (LCA) at the edge, which will reduce the lateral FF divergences.[19,20] In addition, the fabricated grooves (Regions III and V) will also increase the losses of high-order lateral modes and reduce the number of lasing modes.[14] As expected, a narrower range of NF intensity of the LLGS laser can be obtained, as shown in the inset of Fig. 2.

In the epitaxial direction, the active region consists of two 11 nm $GaAs_{0.86}P_{0.14}$ QWs with a 10 nm $Al_{0.4}Ga_{0.6}As$ barrier emitting at 808 nm, and is embedded in the optical defect layers. The photonic crystal waveguide contains 10 periods of $Al_{0.5}Ga_{0.5}As/Al_{0.35}Ga_{0.65}As$ alternating low- and high-index layers on the p and n sides respectively, and all interfaces are linearly graded in composition throughout the thickness of 20 nm to reduce the electrical resistance. The total epitaxial thickness of the PBC structure is 14.8 μm. More detail can be found in Ref. 5.

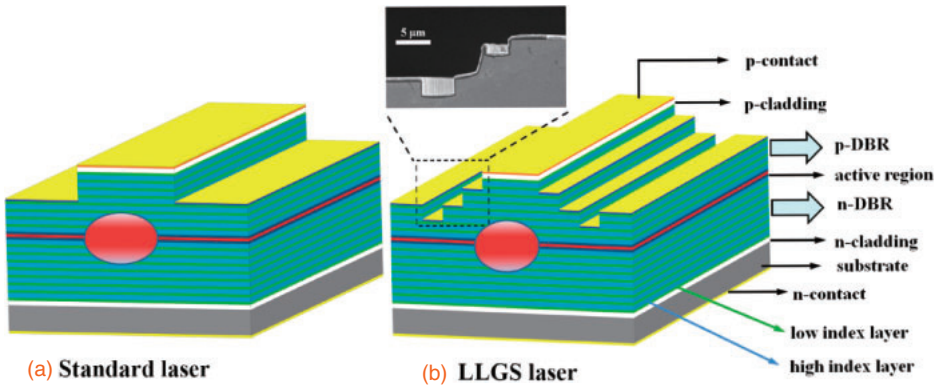

Fig. 1. Schematic diagrams of standard PBC laser and LLGS PBC laser. The inset is a SEM image of the fabricated LLGS.

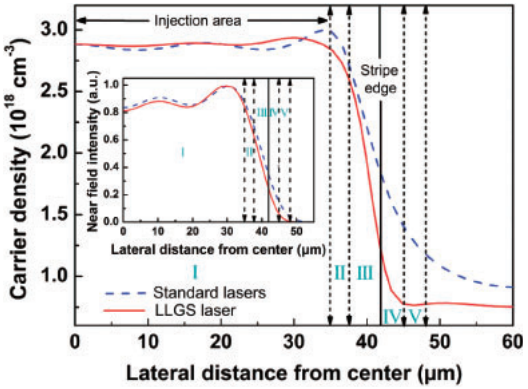

Fig. 2. Lateral carrier profiles of upper QW in the LLGS (dashed line) and standard (solid line) lasers at 1.5 A injection current. The inset shows the NF intensity profile for these two lasers.

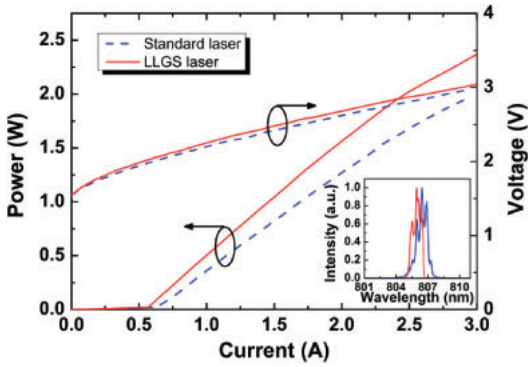

Fig. 4. Emission power (left axis) and voltage (right axis) versus current in the standard laser and LLGS laser. The inset shows the lasing spectra of the standard laser (blue dashed line) and LLGS laser (red line) at 1 W output power.

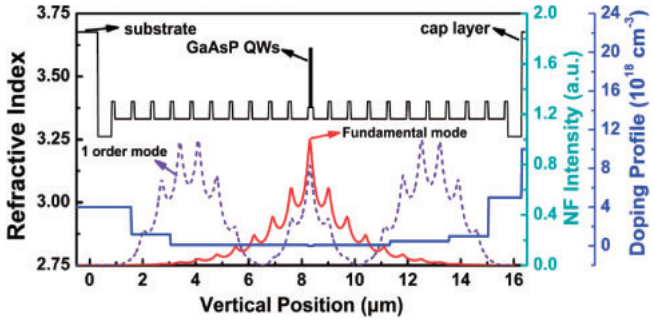

Fig. 3. Refractive index profile, doping profile, and optical field distribution for fundamental mode (red solid line) and first-order mode (violet dashed line) of PBC lasers along epitaxial direction.

Figure 3 shows the refractive index distribution, calculated NF profiles of the fundamental mode and the first-order mode, and the doping profile. It is obvious that the fundamental mode is localized with its maximum in the active region and decays away from it. Compared with the fundamental mode, the first high-order mode leaks to the whole waveguide and penetrates into the substrate and contact layer. Hence, the high-order mode will suffer high loss and low modal gain. In addition, the refractive index step of high- and low-index layers in this PBC waveguide is as high as 0.07, so a stable fundamental mode is easily realized.[21,22)]

The epitaxial layers were grown on a (100)-oriented, n+ GaAs substrate by Aixtron-200 metal–organic chemical vapor deposition (MOCVD). After epitaxial growth, the samples were patterned into LLGS BA stripe lasers by standard processing. An 84-μm-wide stripe was defined first with an etching depth of 4.5 μm by inductively coupled plasma (ICP) etching. In accordance with the simulated results described in context, 4.5- and 4-μm-wide grooves were fabricated synchronously and symmetrically on both sides of the stripe by one-step lithography and etching. The 4.5-μm-wide grooves are located at the edge of a stripe, and the grooves of 4 μm are located at the bottom of the stripe with a distance of 3 μm from the stripe edge. The depth for these grooves was 2 μm. Hence, the LLGS was realized. Then a 300 nm SiO_2 coating was deposited for electrical insulation. A P-contact window with a width of 70 μm was opened and a metallic Ti–Pt–Au ohmic contact was deposited by magnetron sputtering. After wafer thinning and polishing, the thickness of the sample was reduced to 150 μm, and lastly, n-type metal Au–Ge–Ni was grown. Finally, the wafer was cleaved into single devices with a cavity length of 1.7 mm. The devices were mounted on indium-coated *c*-mounts directly for testing without facet passivation or coating. For comparison, standard devices without the LLGS but with the same cavity length and stripe width were fabricated on the same sample.

Figure 4 presents the measured light–current–voltage (*L*–*I*–*V*) curves of the BA PBC lasers with and without the LLGS at the heat-sink temperature of 25 °C. Under the continuous-wave (CW) operation, the threshold current of the LLGS PBC laser is 0.57 A, which is 9.5% lower than that of the standard device. The series resistance of the LLGS device is higher than that of the standard device, but the maximum

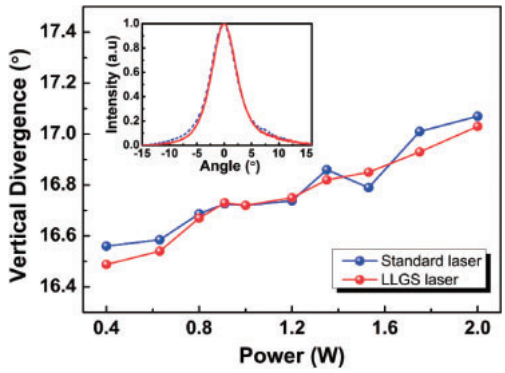

Fig. 5. Vertical FF divergence for 95% power content against power for the LLGS laser and the standard laser. The inset shows the detailed FF profiles of these two types of lasers at the power of 2 W.

power from two facets is improved by 15.4%. Accordingly, the slope efficiency of the LLGS laser is improved by 17.4% compared with the standard laser (~0.76 W/A). The decreased threshold current might be due to the improved internal injection efficiency[23] attributed to the tailored current injection by the LLGS in BA PBC lasers. The inset shows the lasing spectra for these two devices at 1 W output power. The spectrum width of the LLGS laser containing 95% of the power is 1.3 nm, which is narrower than that of the standard laser (~2.17 nm). The narrower spectrum of the LLGS laser might be due to the decreased number of lateral high-order modes.[24]

The dependence of the vertical FF divergence on the output power is plotted in Fig. 5 for these two devices. Almost the same dependence on the power is shown, which is reasonable because the LLGS affects only the lateral FF and the vertical FF is determined by the PBC structure in the epitaxial direction. The vertical divergences are quite stable in the whole current range and increase by no more than 0.52°, which reflects the high stability of the fundamental transverse-mode operation of PBC lasers. The inset shows the FF profile at 2 W. The corresponding divergences for 95% power content ($\theta_{\perp,95\%}$) are, respectively, 16.5 and 16.7° for the LLGS lasers and standard lasers.

The lateral NF and FF intensity profiles at the CW power of 2 W were measured and are shown in Fig. 6. The NF profile testing was performed using a Cincam CMOS-1202 laser beam profile with a 20× microscope objective. The evident improvement in the NF of the lasers as a result of introducing the LLGS can be seen in Fig. 6(a), where the LLGS device shows a steeper and narrower range of NF intensity profile than that of the standard laser. The beam waist is about 86 μm for the LLGS laser at 2 W. In contrast, the value for the standard laser is 91 μm under the same condition. The corresponding improvement is about 5%, which is almost the same as the value (~4%) predicted from the calculated NF. This phenomenon might be a potential reason for the lower threshold current and higher output power in LLGS lasers because the narrow NF means an enhanced overlap between the optical field and the gain medium. Figure 6(b) shows the lateral FF profiles of these two devices at 2 W. An obvious narrower divergence is evident for the LLGS laser. The corresponding $\theta_{\parallel,95\%}$ is, respectively, 12 and 9.5° for the standard device and the LLGS device, which means a decrease of 20.8% in $\theta_{\parallel,95\%}$ owing to the LLGS. Meanwhile, the LLGS

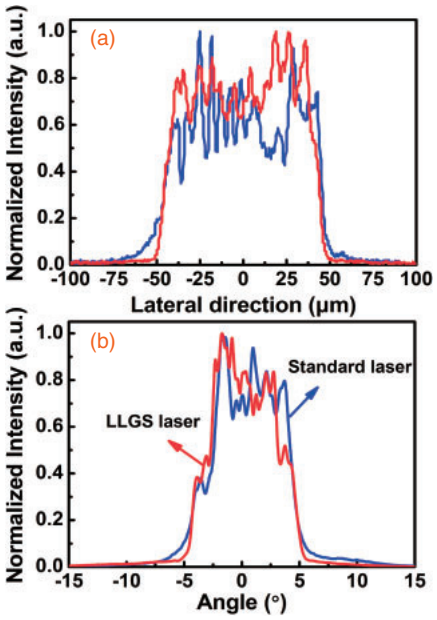

Fig. 6. Measured lateral (a) NF and (b) FF profiles of the LLGS and standard lasers at 25 °C with a CW power of 2 W.

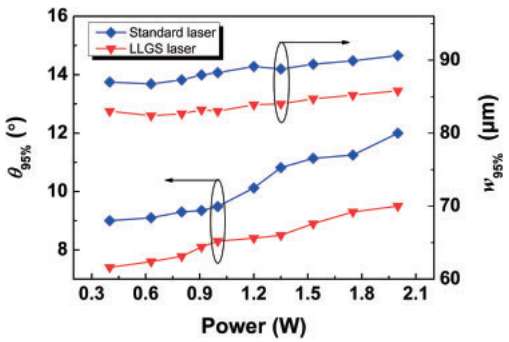

Fig. 7. Measured $w_{95\%}$ and $\theta_{95\%}$ versus output power of standard laser (blue) and LLGS laser (red).

also reduces the dependence of lateral divergence on the injected current. The increment rate for the standard device is 1.26°/A, but this value is only 0.78°/A for the LLGS device, which can be attributed to the decreased LCA.[19,20]

To comprehensively characterize the function of the LLGS in the BA PBC lasers, the beam quality must be obtained. In the vertical direction, the divergence is almost unaffected by the LLGS, so here, we just calculate the lateral beam quality. The lateral beam quality of diode lasers is typically expressed in terms of a lateral beam parameter product (BPP_{lat}), which can be defined as[25]

$$BPP_{\mathrm{lat}} = \frac{w_{95\%}\theta_{95\%}}{4}. \quad (1)$$

Here, $w_{95\%}$ and $\theta_{95\%}$ are the lateral beam-waist diameter and the FF divergence angle containing 95% of the power, respectively. A low BPP_{lat} value is desired for high beam quality since it means more power can be utilized. $w_{95\%}$ and $\theta_{95\%}$ can be obtained from the measured NF and FF results. Figure 7 shows the measured $w_{95\%}$ and $\theta_{95\%}$ of the standard laser and LLGS laser. The decrease in $\theta_{95\%}$ is about 17.7% at a low emission power and 20.8% at a high emission power, which is much better than the improvement in $w_{95\%}$, which is only 5%. The obtained lateral BPP from Eq. (1) is plotted in

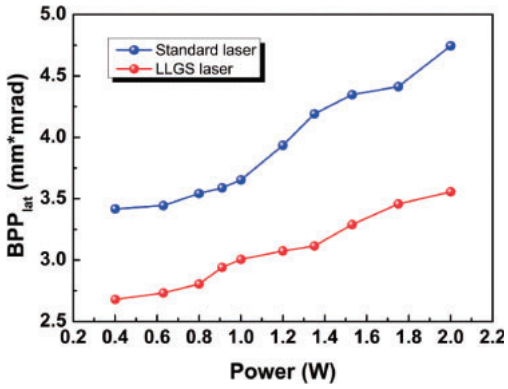

Fig. 8. Lateral BPP as a function of output power for standard laser (blue) and LLGS laser (red).

Fig. 8 as a function of output power. The lateral BPP of the LLGS laser is much lower than that of the standard device. At 0.4 W output power, the BPP value for the LLGS laser is about 2.68 and 3.42 mm·mrad for the standard device. When the power reaches 2 W, the BPP_{lat} of the LLGS laser is as low as 3.55 mm·mrad, corresponding to an improvement of 25.2% compared with the standard laser. This result is much better than in our previous work,[13] in which about 15.9% improvement in the lateral BPP and 4.6% improvement in the power were realized by adopting the fish-bone microstructure in the same PBC lasers.

In summary, the improved threshold, NF, emission power, and beam quality were demonstrated in BA PBC lasers with the LLGS. A power increase of 15.4% and a decrease of 25.2% in the lateral BPP were shown. The underlying mechanism was investigated and found to be related to the decrease in LCA. We believe that our results will contribute to the development of high-power, low-divergence PBC diode lasers.

Acknowledgments This study was supported by the National Natural Science Foundation of China (61404138 and 61474119), National Basic Research Program of China (2013CB933303), Jilin Provincial Natural Science Foundation (20160101243JC and 20150520105JH), and the Opened Fund of the State Key Laboratory on Integrated Optoelectronics (No. IOSKL2016KF15).

1) K. Posilovic, T. Kettler, V. Shchukin, N. Ledentsov, U. Pohl, D. Bimberg, J. Fricke, A. Ginolas, G. Erbert, and G. Tränkle, Appl. Phys. Lett. **93**, 221102 (2008).
2) L. Liu, H. W. Qu, Y. Liu, Y. J. Zhang, Y. F. Wang, A. Y. Qi, and W. H. Zheng, Appl. Phys. Lett. **105**, 231110 (2014).
3) C. Z. Tong, B. J. Bijlani, L. J. Zhao, S. Alali, Q. Han, and A. S. Helmy, IEEE Photonics Technol. Lett. **23**, 1025 (2011).
4) L. J. Wang, Y. Yang, Y. G. Zeng, C. Z. Tong, X. N. Shan, H. X. Zhao, R. Wang, and S. F. Yoon, Appl. Phys. B **107**, 809 (2012).
5) L. Wang, C. Tong, S. Tian, S. Shu, Y. Zeng, J. Rong, H. Wu, E. Xing, Y. Ning, and L. Wang, IEEE J. Sel. Top. Quantum Electron. **21**, 343 (2015).
6) D. Mehuys, R. Lang, M. Mittelstein, J. Salzman, and A. Yariv, IEEE J. Quantum Electron. **23**, 1909 (1987).
7) B. Sumpf, K.-H. Hasler, P. Adamiec, F. Bugge, F. Dittmar, J. Fricke, H. Wenzel, M. Zorn, G. Erbert, and G. TrÄnkle, IEEE J. Sel. Top. Quantum Electron. **15**, 1009 (2009).
8) D. Heydari, Y. Bai, N. Bandyopadhyay, S. Slivken, and M. Razeghi, Appl. Phys. Lett. **106**, 091105 (2015).
9) H.-C. Eckstein and U. D. Zeitner, Opt. Express **21**, 23231 (2013).
10) H.-C. Eckstein, U. D. Zeitner, A. Tünnermann, W. Schmid, U. Strauss, and C. Lauer, Opt. Lett. **38**, 4480 (2013).
11) H. Wenzel, P. Crump, J. Fricke, P. Ressel, and G. Erbert, IEEE J. Quantum Electron. **49**, 1102 (2013).
12) N. Stelmakh, Proc. SPIE **7230**, 72301B (2009).
13) J. M. Rong, E. B. Xing, L. J. Wang, S. L. Shu, S. C. Tian, C. Z. Tong, and L. J. Wang, Appl. Phys. Express **9**, 072104 (2016).
14) H. An, Y. Xiong, C.-L. Jiang, B. Schmidt, and G. Treusch, Proc. SPIE **8965**, 89650U (2014).
15) T. Wang, C. Z. Tong, L. J. Wang, Y. G. Zeng, S. C. Tian, S. L. Shu, J. Zhang, and L. J. Wang, Appl. Phys. Express **9**, 112102 (2016).
16) LASTIP (Crosslight Software Inc., Burnaby, BC, 2010) [www.crosslight.com].
17) J. Houlihan, J. O'Callaghan, V. Voignier, G. Huyet, J. McInerney, and B. Corbett, Opt. Lett. **26**, 1556 (2001).
18) P. C. R. Gurney and R. F. Ormondroyd, IEEE J. Quantum Electron. **31**, 427 (1995).
19) J. Piprek and Z. S. Li, Appl. Phys. Lett. **102**, 221110 (2013).
20) M. Winterfeldt, P. Crump, S. Knigge, A. Maaßdorf, U. Zeimer, and G. Erbert, IEEE Photonics Technol. Lett. **27**, 1809 (2015).
21) M. J. Miah, T. Kettler, V. P. Kalosha, K. Posilovic, D. H. Bimberg, J. Pohl, and M. Weyers, IEEE J. Sel. Top. Quantum Electron. **21**, 722 (2015).
22) C. Z. Tong, B. J. Bijlani, S. Alali, and A. S. Helmy, IEEE J. Quantum Electron. **46**, 1605 (2010).
23) P. Crump, P. Leisher, T. Matson, V. Anderson, D. Schulte, J. Bell, J. Farmer, M. DeVito, R. Martinsen, and Y. Kim, Appl. Phys. Lett. **92**, 131113 (2008).
24) G. Lengyel, H. D. Wolf, and K. H. Zschauer, J. Appl. Phys. **49**, 1047 (1978).
25) M. Winterfeldt, P. Crump, H. Wenzel, G. Erbert, and G. Tränkle, J. Appl. Phys. **116**, 063103 (2014).